Mechanism of the Kinetically-Controlled Folding Reaction of Subtilisin†

Kathryn E. Fisher, Biao Ruan, Patrick A. Alexander, Lan Wang, and Philip N. Bryan*

Center for Advanced Research in Biotechnology, University of Maryland Biotechnology Institute, 9600 Gudelsky Drive, Rockville, Maryland 20850

Received August 7, 2006; Revised Manuscript Received November 13, 2006

ABSTRACT: Like many secreted proteases, subtilisin is kinetically stable in the mature form but unable to fold without assistance from its prodomain. The existence of high kinetic barriers to folding challenges many widely accepted ideas, namely, the thermodynamic determination of native structure and the sufficiency of thermodynamic stability to determine a pathway. The purpose of this article is to elucidate the physical nature of the kinetic barriers to subtilisin folding and to show how the prodomain overcomes these barriers. To address these questions, we have studied the bimolecular folding reaction of the subtilisin prodomain and a series of subtilisin mutants, which were designed to explore the steps in the folding reaction. Our analysis shows that inordinately slow folding of the mature form of subtilisin results from the accrued effects of two slow and sequential processes: (1) the formation of an unstable and topologically challenged intermediate and (2) the proline-limited isomerization of the intermediate to the native state. The low stability of nascent folding intermediates results in part from subtilisin's high dependence on metal binding for stability. Native subtilisin is thermodynamically unstable in the absence of bound metals. Because the two metal binding sites are formed late in folding, however, they contribute little to the stability of folding intermediates. The formation of productive folding intermediates is further hindered by the topological challenge of forming a left-handed crossover connection between β-strands S2 and S3. This connection is critical to propagate the folding reaction. In the presence of the prodomain, folding proceeds through one major intermediate, which is stabilized by prodomain binding, independent of metal concentration and proline isomerization state. The prodomain also catalyzes the late proline isomerizations needed to form metal site B. Rate-limiting proline isomerization is common in protein folding, but its effect in slowing subtilisin folding is amplified because of the instability of the intermediate and an apparent need for simultaneous isomerization of multiple prolines in order to create metal site B. Thus, the kinetically controlled folding reaction of subtilisin, although unusual, is explained by the accrued effects of events found in other proteins.

Extracellular proteases are synthesized as pro-enzymes, perhaps as a result of a biological imperative for the tight regulation of protease activation (*1*). The mature forms of these proteases can manifest usual folding behavior (*2*). The mature protease can be stable in a practical sense. That is, the native conformation persists under favorable solvent conditions for months or more. Yet, once denatured and returned to these same favorable conditions, it can remain in an unfolded conformation for months or more. The existence of high kinetic barriers to folding challenges many widely accepted ideas, namely, the thermodynamic determination of native structure and the sufficiency of thermodynamic stability to determine a pathway (*3*). Thus, the evolution of pro-proteins as folding units appears to have created kinetically controlled folding mechanisms that are different from the mechanisms for facile-folding proteins (*4*).

Subtilisin BPN′ is a serine protease secreted from the soil bacterium *Bacillus amyloliquefaciens*. It is produced *in vivo* from a pre-pro-protein (*5*, *6*). The 30 amino acid presequence serves as a signal peptide for protein secretion across the membrane and is hydrolyzed by a signal peptidase (*7*). The extracellular part of the maturation process involves folding of prosubtilisin, self-processing of the 77 amino acid prodomain to produce a processed complex, and finally degradation of the prodomain to create the 275 amino acid mature form of the enzyme (*8*, *9*). The prodomain will catalyze folding of the mature form of the protease even as a separate polypeptide chain. Examples of prodomain mediated folding have been found in all four mechanistic families of proteases: serine proteases (*10*−*17*), including the eukaryotic prohormone convertases, which are structural homologues of bacterial subtilisin (*18*−*22*); aspartic proteases (*23*−*25*); metalloproteases (*26*−*30*) and cysteine proteases (*31*).

In spite of a great deal of careful quantitative work in the area, there has yet been no satisfactory explanation as to the cause of the inordinately high kinetic barrier to subtilisin folding. This article seeks to answer the two fundamental questions pertaining to catalyzed folding: (1) what are the kinetic barriers between the unfolded and native states of subtilisin and (2) how does the prodomain reduce these kinetic barriers? To address these questions, we have studied the bimolecular folding reaction of denatured subtilisin and prodomain. The product of bimolecular folding is a stable

† This work was supported by NIH Grant GM42560.

* Corresponding author. Tel: 240-314-6220. Fax: 240-314-6255. E-mail: bryan@umbi.umd.edu.

10.1021/bi061600z CCC: $37.00
Published on Web 12/21/2006

complex between the native protease and the prodomain. The native complex has been characterized both by X-ray crystallography (*32*, *33*) and NMR studies (the article following this one).

Several properties of subtilisin make quantitative investigation of the folding reaction difficult and necessitate the use of various mutants to facilitate study. First, folding studies must be carried out on mutants that have little proteolytic activity. This is necessary so that the reactants are not degraded in the course of an experiment. A more serious challenge, however, is the complexity of the reaction. Multiple linked equilibria need to be unraveled to solve the kinetic puzzle. The basic reaction mechanism for bimolecular folding is as follows, where P is the folded prodomain; P_U is the unfolded prodomain; U is unfolded subtilisin; PI is a collision complex of a partially folded subtilisin and prodomain; N is native subtilisin; and PN is the complex of native subtilisin and prodomain.

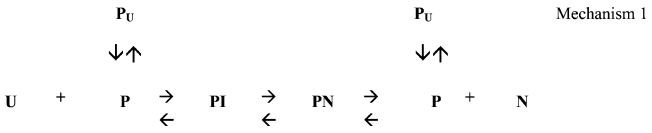

Superimposed upon this basic mechanism is subtilisin's affinity for ions. Native subtilisin contains two metal binding sites. One, called site A, specifically binds calcium (K_a = 10^7 M^{-1} at 25 °C), and the other, called site B, can bind both divalent and monovalvent metals, albeit more weakly. Calcium at site A is coordinated by five carbonyl oxygen ligands and one aspartic acid (Figure 1A). A loop of nine amino acids (75−83) interrupts the last turn of helix C and forms the central part of site A (*34*). The loop is part of a rare left-handed crossover, joining beta strands two and three. Site B is located 32 Å from site A in a shallow crevice comprising connecting loops between β-strands 5 and 6 and 6 and 7 (Figure 1B). In the absence of calcium, this locus will bind a monovalent cation. The K_a of site B is 6.7×10^4 M^{-1} for calcium and 10^4 M^{-1} for potassium at 25 °C (*35*). The binding of ions is mutually exclusive so that as the calcium concentration increases, the monovalent ion is displaced (*36*). At low metal concentration (e.g., 30 mM Tris[1]-HCl at pH 7.4 and 100 μM EDTA) subtilisin is unstable, unfolding at a rate of 0.6 h^{-1} (S221A subtilisin) (*4*). At high metal concentrations (e.g., 0.1 M calcium), binding energy contributes 13.5 kcal/mol to the free energy of unfolding. A complete analysis of metal ion binding to native subtilisin has been presented by Alexander et al. (*35*).

In this article, we analyze the folding reaction of the S221A mutant of subtilisin with a stabilized version of the prodomain, denoted proR9 (*37*). We next analyze the folding reactions of a series of subtilisin mutants in which various steps in the reaction are affected. We finally synthesize the structural and mechanistic information into a comprehensive folding model.

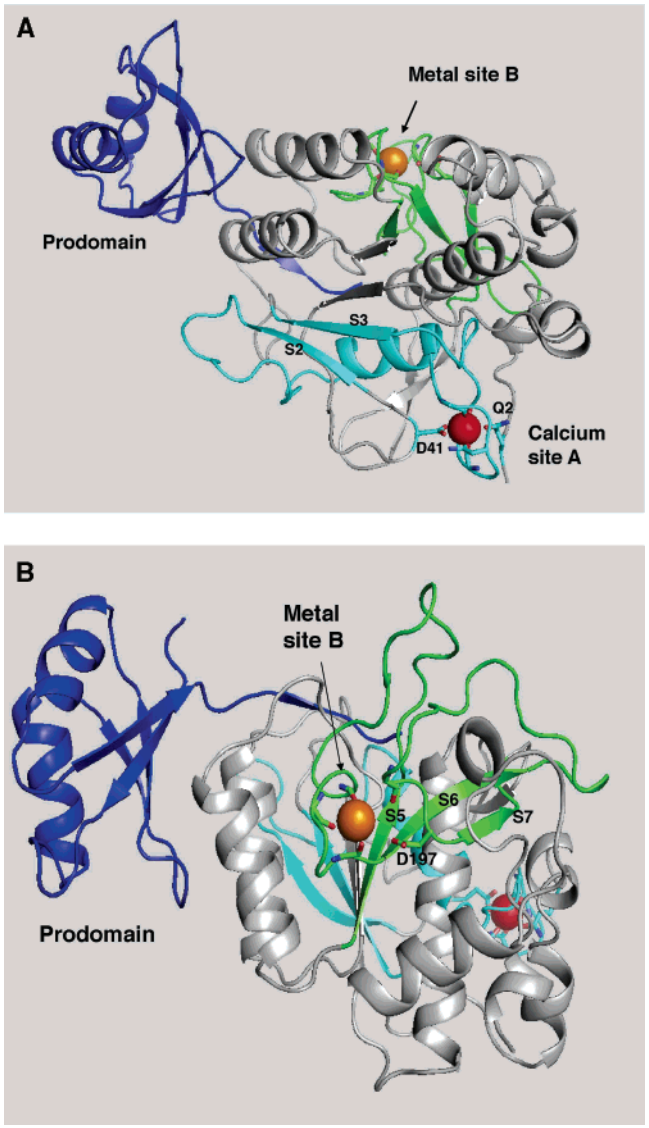

FIGURE 1: (A) Subtilisin−prodomain complex and calcium site A. Ribbon cartoon of the prodomain (blue) (1spb) in complex with subtilisin (1sud). β-strands S2 and S3 and the left-handed crossover connection between them are shown in cyan. The left-handed crossover includes α-helix C and calcium binding site A. Calcium at site A (red sphere) is coordinated by four of the carbonyl oxygen ligands in the 75−83 loop. The bidentate carboxylate (D41)is on the left side of the loop, whereas the *N*-terminus of the protein and the side chain of Q2 are on the right side. Metal site B is shown in the background with a sodium ion depicted as an orange sphere. (B) Subtilisin−prodomain complex and metal site B. Ribbon cartoon of the prodomain (blue) (1spb) in complex with subtilisin (1sud). β-strands S5, S6, and S7 and the two connecting loops are shown in green. The connecting loops contain the ligands bound to a sodium (orange sphere) at site B: the carboxylate oxygen of D197 and the carbonyl oxygen atoms of G169, Y171, V174, and E195. Calcium site A is shown in the background with the calcium ion depicted as a red sphere (*36*).

MATERIALS AND METHODS

Fermentation and Purification of Subtilisin from B. subtilis. Inactive mutants of subtilisin BPN′ were expressed in *B. subtilis* in a 1.5 l New Brunswick fermentor with 1 μg/mL of the subtilisin variant Sbt184 (Q2K, S3C, P5S, I31L, K43N, M50F, A73L, Δ75-83, E156S, G166S, G169A,

[1] [1]Abbreviations: A shorthand for denoting amino acid substitutions employs the single letter amino acid code as follows: S221A denotes the change of serine 221 to alanine; proR9, subtilisin BPN′ prodomain with the following mutations: the substitution of amino acids 17−21 (TMSTM) with SGIK and the subtitutions A23C, K27E, V37L, Q40C, H72K, and H75K; Sbt70, subtilisin BPN′ with the following mutations: K43N, M50F, A73L, Δ75-83, Q206V, Y217K, N218S, and S221A; Tris, Tris(hydroxymethyl)amino-methane.

Q206C, A216E, K217L, N218S, M222Q, T254A, and Q271E) (*38*) added to the media to facilitate the processing of prosubtilisin. Sbt184 has a pI of ~6 and can be separated by ion-exchange chromatography from active site variants. Variants were expressed at a level of 100−500 mg per liter. Purification was as described (*39*).

Fermentation and Purification of Facile-Folding Subtilisin from E. coli. The mutagenesis and protein expression of inactive Δ75-83 SBT mutants were performed using a vector called pJ1. Vector pJ1 is identical to pG5 (*40*) except that the Cla I site of pG5 has been removed. The SBT gene was inserted between Nde I and Hind III sites in the polycloning site of pJ1 and transformed into *E. coli* production strain BL21(DE3). Subtilisin variants were purified as described (*37*), lyophilized, and stored at −20 °C. The concentration of subtilisin was determined by UV absorbance using 1 mg/mL = A_{280} of 1.17.

Expression of Prodomain Mutant ProR9. The fermentation of the prodomain was carried out in *E. coli* strain BL21-(DE3) as described (*37*). The concentration of proR9 was determined by UV absorbance using 1 mg/mL = A_{275} of 0.67.

Kinetic Analysis of Prodomain Facilitated Subtilisin Folding. Single Mixing. Refolding of subtilisin is accompanied by a 1.5-fold increase in the tryptophan fluorescence of subtilisin upon folding into its complex with the prodomain. There are three tryptophan residues in the subtilisin mutants and none in the prodomain. Reaction kinetics were measured using a KinTek Stopped-Flow Model SF2001 (excitation λ = 300 nm; emission, 340 nm cutoff filter) as described (*41*). A stock solution of subtilisin at a concentration of 100 μM in 50 mM KPi at pH 7.0 was prepared for refolding studies. Subtilisin was denatured by diluting 20 μL of the stock solution into 1 mL of 50 mM HCl. The samples were neutralized by mixing the subtilisin and HCl solution into an equal volume of 60 mM Tris-base at pH 9.4, 100 mM KCl, and the prodomain in the KinTek Stopped-flow (final buffer concentrations were 30 mM Tris-HCl at pH 7.4 and 50 mM KCl). The final concentration of subtilisin was 1 μM, whereas the prodomain concentration was varied from 2.5 to 80 μM. Typically, 5−10 kinetics traces were collected for each prodomain concentration. Reaction kinetics were also monitored using gel filtration on a 30 cm × 1 cm diameter G75 column equilibrated in 30 mM Tris-HCl at pH 7.4 and 50 mM KCl. A stock solution of subtilisin at a concentration of 100 μM in 50 mM KPi at pH 7.0 was prepared for refolding studies. Subtilisin was denatured by diluting 60 μL of the stock solution into 1 mL of 50 mM HCl. The samples were neutralized by mixing the subtilisin and HCl solution into an equal volume of 60 mM Tris-base at pH 9.4, 100 mM KCl, and 40 μM prodomain in a microfuge tube (final buffer concentrations were 30 mM Tris-HCl at pH 7.4 and 50 mM KCl). At time intervals from 3 to 75 min, 0.2 mL of the reaction mix was injected onto the column at a flow rate of 3 mL/min.

Double Jump: Renaturation−Denaturation. The kinetics of the formation of the folded complex, PS, were determined by a double-jump renaturation−denaturation experiment. The KinTek Stopped Flow in the three syringe configuration was used to perform the two mixing steps. In the first mixing step, 3 μM subtilisin in 50 mM HCl is mixed with a variable concentration of prodomain in 60 mM Tris-base and 100 mM KCl. The resulting solution is 30 mM Tris-HCl and 50 mM KCl at pH 7.4. The final concentration of subtilisin was 1.5 μM, whereas the prodomain concentration was varied from 5 to 20 μM after the first mixing step. Subtilisin and prodomain are allowed to fold under native conditions in the delay line of the stopped-flow instrument for aging times ranging from 10 to 1500 s. After the prescribed aging time, the subtilisin−prodomain solution is mixed 2:1 with 0.1 M H_3PO_4 to bring the pH to 2.3. Fluorescence data for the denaturation of the folded complex was collected after the second mixing step. At each renaturation time point, the denaturation curve was fit to a single-exponential decay curve. The amplitude of the decay curve was recorded as a function of refolding time to assess the amount of folded complex that had accumulated at each renaturation time.

Double Jump: Denaturation−Renaturation. A double jump denaturation−renaturation experiment was used to study the effect of denaturation time on the rates and amplitudes of the folding reaction. The KinTek Stopped Flow in the three syringe configuration was used to perform the two mixing steps. In the first mixing reaction, 3 μM subtilisin and 30 μM proR9 in 0.05 M KPi at pH 7.2 was denatured by mixing with an equal volume of 0.1 M phosphoric acid. The resulting solution had a pH of 2.15. The denaturation reaction was aged for varied lengths of time and then mixed with one-half volume of 0.15 M KPO_4 at pH 12.0. The final conditions were 1 μM sbt15 and 10 μM proR9 in 0.1 M KPi at pH 7.2 and 25 °C. The folding process is then followed by fluorescence change.

A second double mixing denaturation−renaturation experiment was used to follow folding kinetics after 0.5 s of denaturation. The two mixing steps were performed using a BioLogic SFM-4 Q/S in the stopped flow mode. In the first step, 2 μM Sbt70 in 10 mM KPi at pH 7.2 is mixed with an equal volume of 100 mM HCl. The resulting solution is 1 μM Sbt70, 50 mM HCl, and 5 mM KPi at pH 2.1. After 0.5 s, the denatured sbt70 solution is mixed with an equal volume of 60 mM Tris-base, 5 mM KPi, and variable amounts of proR9. The resulting solution is 0.5 μM Sbt70, 5−20 μM proR9, 30 mM Tris-HCl, and 5 mM KPi at pH 7.5. The renaturation process is followed by fluorescence change.

Triple Jump: Denaturation−Renaturation−Denaturation. A triple mixing denaturation−renaturation−denaturation experiment was performed to directly measure the accumulation of the native complex after a denaturation time of 0.5 s. The three mixing steps were performed using a BioLogic SFM-4 Q/S in the stopped flow mode. In the first step, 5 μM Sbt70 in 10 mM KPi at pH 7.2 is mixed with an equal volume of 100 mM HCl. The resulting solution is 2.5 μM Sbt70, 50 mM HCl, 5 mM KPi at pH 2.1. After 0.5 s, the denatured sbt70 solution is mixed with an equal volume of 60 mM Tris-base, 5 mM KPi, and 10 μM proR9. The resulting solution is 1.25 μM Sbt70, 5 μM proR9, 30 mM Tris-HCl, and 5 mM KPi at pH 7.5. Sbt70 and proR9 are allowed to fold under native conditions in the delay line for aging times ranging from 0.5 to 60 s. After the prescribed aging time, the Sbt70−proR9 solution is mixed 3:1 with 0.132 M H_3PO_4 to bring the pH to 2.3 and denature the folding reaction. At each renaturation time point, the denaturation curve was fit to a single-exponential decay curve. The amplitude of the decay curve was recorded as a

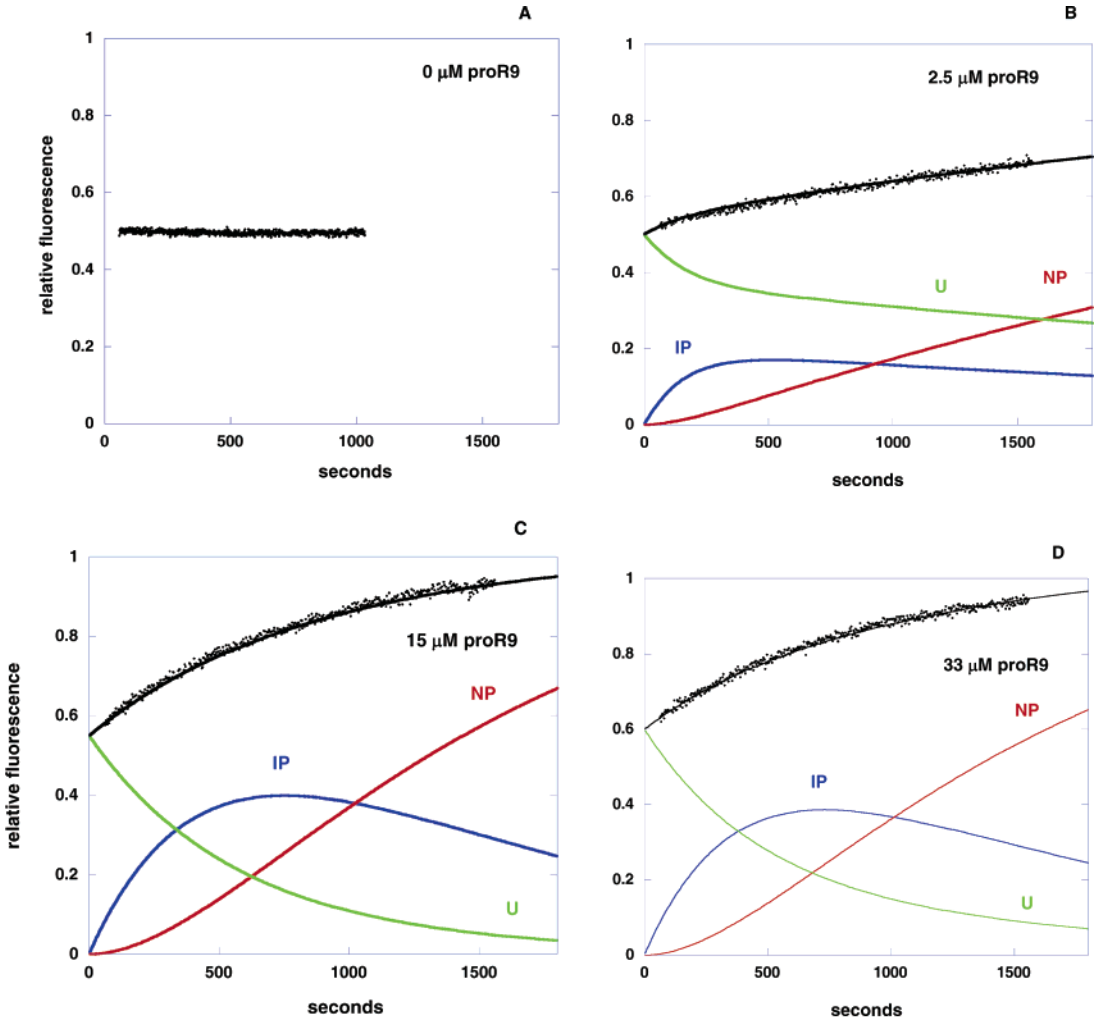

FIGURE 2: Folding rate of S221A subtilisin in the presence of proR9. ProR9 and 1 μM denatured subtilisin were mixed in 30 mM Tris-HCl at pH 7.4 and 50 mM KCl at 25 °C. The reaction was followed by an increase in tryptophan fluorescence, which occurs upon the folding of subtilisin into the prodomain−subtilisin complex. The experimental data were fit to mechanism 2 using KinSim (*55*). The fit is shown by the solid black line which shows the sum of the fluorescence of U + IP + NP. The concentrations of proR9 were as noted in the Figure panels.

function of refolding time to assess the amount of folded complex that had accumulated at each renaturation time.

RESULTS AND DISCUSSION

Folding of S221A Subtilisin as a Function of Prodomain Mutant ProR9. Bimolecular folding of subtilisin with the wild type prodomain is very slow (~0.2 s^{-1} M^{-1} of the prodomain) (*42*). The slow time scale of folding makes detailed kinetic analysis of the process problematic. To overcome this dilemma, it was necessary to create a mutant prodomain that was a more effective folding catalyst. We were able to accomplish this by understanding the relationship between the independent stability of the prodomain and its ability to facilitate subtilisin folding. In complex with subtilisin, the prodomain folds into a stable compact structure, comprising a four-stranded antiparallel β-sheet and two three-turn α-helices (Figure 1A and B). When isolated from subtilisin, the prodomain is 97% unfolded even under optimal folding conditions (*41*). This low stability is likely of biological relevance to ensure that the prodomain−subtilisin complex exists only transiently and that the mature protease is released expeditiously in active form. The wild type prodomain is relatively inefficient in catalyzing bimolecular folding, however, because only the folded form of the prodomain is active. We thus created a prodomain (denoted proR9) that is stably folded when isolated from subtilisin ($\Delta G_{folding}$ = −4 kcal/mol) (*37*, *43*). ProR9 has no mutations that directly affect its contact surface with subtilisin but is much more efficient in catalyzing subtilisin folding because of its independent stability. ProR9 not only effectively removes the P_U/P equilibrium from the overall reaction scheme (mechanism 1) but also accelerates subtilisin folding to a practical experimental time scale (h^{-1}).

Figure 2 shows the refolding kinetics of S221A subtilisin (1 μM) with an excess of proR9 (2.5−33 μM) in 30 mM Tris-HCl and 50 mM KCl at pH 7.4 and 25 °C. The folding reaction was followed both by manual mixing and stopped flow mixing to make certain that all kinetic components were observed. The rates and amplitudes of fluorescence changes during a single turnover of subtilisin folding were measured. ProR9 does not have tryptophan residues, and therefore, the fluorescence increase observed above 345 nm upon excitation at 300 nm is almost entirely due to the burial of the 3 tryptophans in subtilisin. Fluorescence traces approximated single-exponential growth. This experiment gives no indication that any intermediate accumulates in the course of the

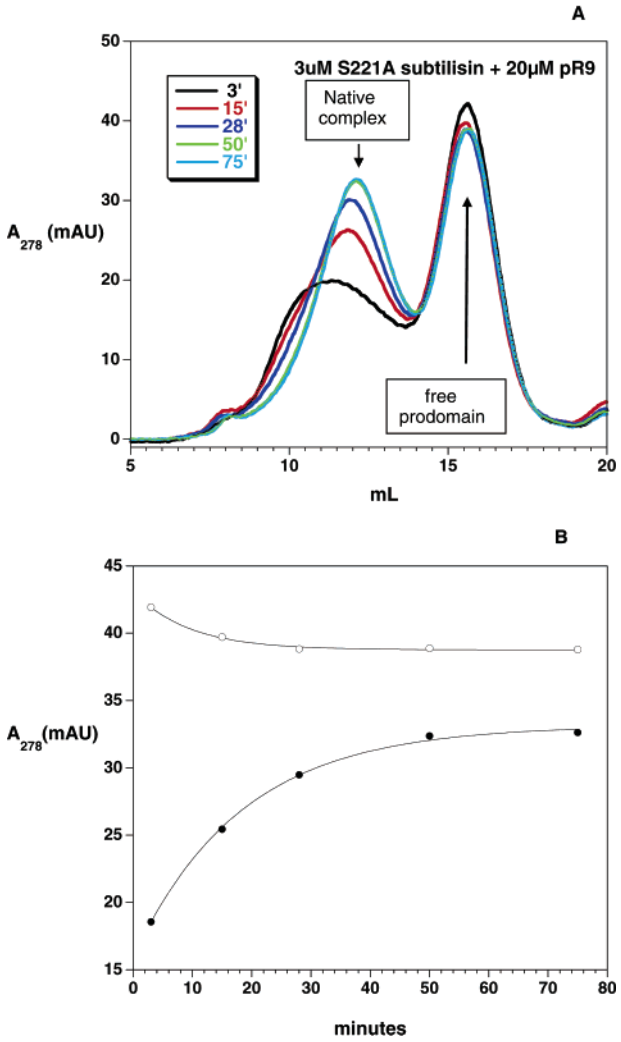

FIGURE 3: (A) Folding rate of S221A subtilisin and proR9 followed by gel filtration. Twenty micromolar proR9 and 3 μM denatured Sbt70 were mixed in 30 mM Tris-HCl at pH 7.4 and 50 mM KCl at 25 °C. The reaction was followed by injecting the reaction mix onto a G75 column at time intervals from 3 to 75 min. In the course of the reaction, the concentrations for free proR9 (15.7 mL elution) decreases, and the concentration of the native complex (12.5 mL elution) increases. (B) Folding rate of S221A subtilisin and proR9 followed by gel filtration. The peaks for free proR9 (15.7 mL peak from part A, ○) and the native complex (12.5 mL peak from part A, ●) are plotted vs folding time. The decrease in proR9 concentration is fitted to a single-exponential equation with a rate constant of 0.0017 s^{-1}, and the accumulation of [PN] is fitted to a single-exponential equation with a rate constant of 0.0008 s^{-1}.

folding reaction. For numerous mutants, however, a bimolecular intermediate complex becomes highly populated (see below). To resolve the kinetics steps for the formation of the intermediate (PI) from the isomerization of PI to PN, we performed gel filtration experiments. The S221A subtilisin folding reaction is slow enough (h^{-1}) to make gel filtration a useful method with which to simultaneously measure the decrease of unfolded subtilisin, the decrease of free prodomain, and the accumulation of native complex. The results of mixing 3 μM denatured S221A subtilisin with 20 μM proR9 are shown in Figure 3A. The gel filtration results show that the reaction occurs in at least two steps, although the two steps occur at similar rates. The rate of proR9 binding can be monitored by the decrease in the elution peak for unbound proR9 at 15.7 mL (Figure 3A). The rate of formation of PN can be monitored by the increase in the elution peak for the native complex at 12.5 mL. ProR9 binding occurs at a rate of 0.0017 s^{-1}, whereas the rate of PN formation is about 2-times slower (0.0008 s^{-1}) (Figure 3B). This reveals that PI accumulates during the reaction. Furthermore, by performing the gel filtration experiment as a function of proR9 concentration from 3 to 15 μM, we determined that the rate of binding was independent of proR9 concentration and that the overall equilibrium constant for proR9 binding ($k_1k_2/k_{-1}k_{-2}$) is 1.4×10^5 M^{-1}. This behavior indicated that although the bimolecular intermediate itself is relatively stable, U must undergo a slow conformational change to a U′ state prior to binding.

In summary, we were able to determine the following: (1) The rate of isomerization of U to U′ (k_1) is 0.0017 s^{-1}. (2) The rate of isomerization of PI to PN (k_3) is 0.001 s^{-1}. (3) The overall equilibrium constant for proR9 binding ($k_1k_2/k_{-1}k_{-2}$) is 1.4×10^5 M^{-1}. (4) The equilibrium constant for U to U′ (k_1/k_{-1}) is ≤ 0.05. (A larger value would lead to an observable population with rapid binding kinetics.) (5) As a result of the above, the equilibrium constant for proR9 binding to U′ (k_2/k_{-2}) is $\geq 3 \times 10^6$ M^{-1}.

Given parameters 1−5 (above), the best fit of all fluorescence and gel filtration data was the following mechanism.

$k_1 = 0.0017s^{-1}$ $k_2/k_{-2} = 1.4 \times 10^7 M^{-1}$ $k_3 = 0.001s^{-1}$

$$U \rightleftarrows I + P \rightleftarrows PI \rightleftarrows PN$$

Mechanism 2

$k_{-1} = 0.17s^{-1}$ $k_{-3} < 10^{-7} s^{-1}$

The fluorescence signal of U at 300 nm is 50% of the signal of PN. The fluorescence signal of PI is 85% of the signal of PN. The fluorescence signal of P at 300 nm is small but creates some background fluorescence signal at high P concentration. The data in Figure 2 were fit to mechanism 2 to calculate the concentrations of reactants, intermediates, and products over the course of the reactions. The experimental data closely fit the calculated fluorescence signal for U + IP + NP at all proR9 concentrations (Figure 2 B−D). Bimolecular folding, therefore, occurs in two slow steps: slow conformational change preceding prodomain binding and slow isomerization of the intermediate complex to the native state. Although the rate of binding of P to U′ is masked by the slow conformational exchange between U and U′, the bimolecular intermediate complex itself is relatively stable with a K_D ($k_{-1}k_{-2}/k_1k_2$) = 7 μM. The native complex is very stable with a K_D of ~0.1 nM (article following this one). For this reason, the dissociation of PN into P + N is omitted in mechanism 2 because tight binding essentially creates a single turn over reaction with PN as the end product. The rate of unfolding of PN into PI (k_{-3}) is small, and its value was estimated on the basis of the H−D exchange rates of amide protons involved in the PI to PN equilibrium (see accompanying article). Mechanism 2 explains why subtilisin folding with the wild type prodomain is so slow. The wild type prodomain binds 100-times slower than proR9. As a result, the overall rate of the reaction falls from 0.0005 s^{-1} in 10 μM proR9 to 1.4×10^{-6} s^{-1} for 10 μM wild type prodomain.

Influence of Metal Concentration on Folding Kinetics. We next investigated whether the kinetics of the reaction were influenced by metal ions. The reaction kinetics were mea-

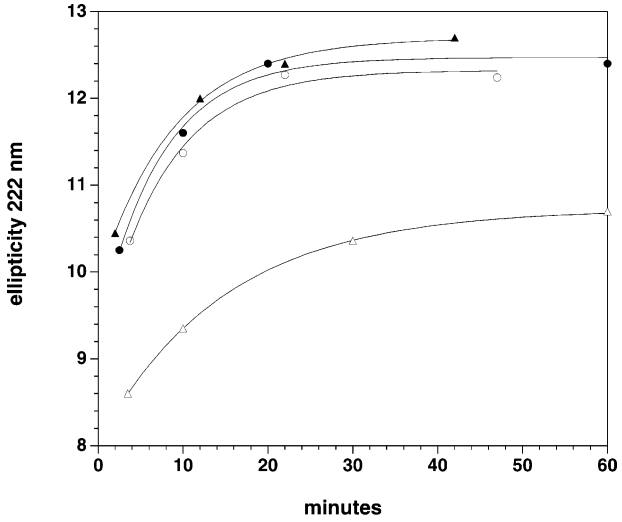

FIGURE 4: Folding rate of S221A subtilisin and proR9 in the presence of different cations. ProR9 (8.5 μM) and 4 μM denatured Sbt70 were mixed in 30 mM Tris-HCl at pH 7.4 at 25 °C ± various cations. The reaction was followed by circular dichroism (CD). A CD spectrum was recorded at each time point in a 0.1 cm path cuvette. The following are shown at the CD values at 222 nm: △, 100 μM EDTA; ▲, 50 mM KCl and 100 μM EDTA; ●, 50 mM KCl and 100 μM $CaCl_2$; and ○, 50 mM KCl and 10 mM $CaCl_2$.

sured in 30 mM Tris-HCl at pH 7.4 with (1) 50 mM KCl and 100 μM EDTA; (2) 50 mM KCl and 100 μM $CaCl_2$; (3) 50 mM KCl and 10 mM $CaCl_2$; (4) 100 μM EDTA and no metal. Folding kinetics were similar in 100 μM EDTA, 100 μM calcium, and 10 mM $CaCl_2$ (with 50 mM KCl). At very low metal concentration (Tris-HCl at pH 7.4 and 100 μM EDTA), however, the reaction proceeded to a partially folded form but did not isomerize to the native PN form (Figure 4). The results indicate that metal ion sites are not formed until late in folding and, therefore, do not influence the kinetics of folding to the intermediate complex. The CD and fluorescence signals for the partially folded state formed at low metal concentration are consistent with the PI state observed in the kinetic experiments. This may indicate that in the absence of all metals, the PI form is more stable than the PN form, and hence, the reaction stops at the PI state. As stated earlier, S221A subtilisin in unstable at low metal concentration, unfolding at a rate of 0.6 h^{-1}.

Influence of Active Site Mutations on Folding Kinetics. We next investigated how various active site mutations influence folding kinetics. Three variations were used in addition to S221A: (1) S221C; (2) N155L; (3) D32N. Folding kinetics of S221C and N155L were very similar to that of S221A. In native subtilisin, S221 is hydrogen bonded to two ordered water molecules (*44*). In S221C subtilisin, the cysteine is easily oxidized. Both the reduced (S−H) and oxidized forms of S221C subtilisin fold with similar rates. In native subtilisin, N155 is hydrogen bonded to both the main chain nitrogen and side chain oxygen of T220. In the L155 mutant, these hydrogen bonds are lost (*45*). None of these perturbations to the native structure have a significant influence on the rate of subtilisin folding.

In contrast, the D32N mutant did not appear to fold at all in the presence of proR9. In native subtilisin, D32 forms a strong hydrogen bond with Nδ1 of the catalytic H64 at the end of helix C (*46*). In the D32N mutant, this interaction is disrupted, and H64 swings out of its normal position into a

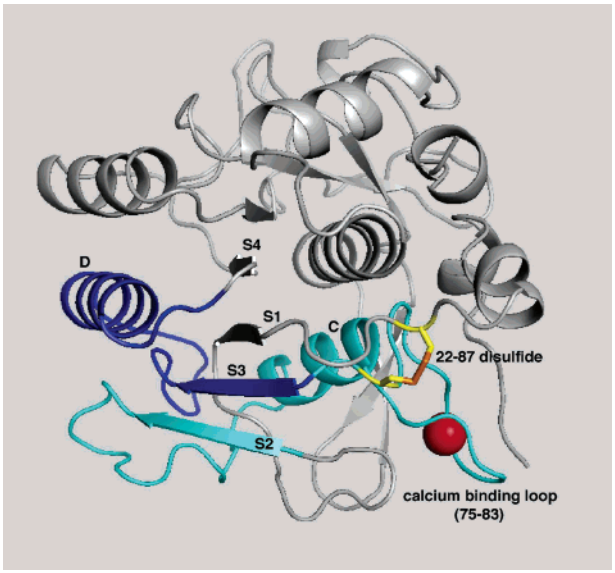

FIGURE 5: Left-handed crossover connection in subtilisin. The subtilisin Cα ribbon is shown in gray (pdb identifier: 1A2Q). The β-strand S2 and the left-handed crossover connection to strand S3 are shown in cyan. The left-handed crossover includes α-helix C and the calcium binding loop (75−83) of site A. Bound calcium at site A is shown as a red sphere. For comparison, β-strand S3 and the right-handed crossover connection to strand S4 are shown in blue. The right-handed crossover includes α-helix D. The disulfide cross-link between amino acids 22 and 87 linking strands S1 and S3 is shown in yellow.

solvent-exposed position (*32*). H64 assumes this position in both the free enzyme and in complex with the prodomain. The loss of the H bond between β-strand S1 and H64 has major effects on the folding reaction. These effects will be described below.

Left-Handed Cross Over: Effect of the C22−C87 Disulfide. We next investigated whether a left handed crossover between β-strands S2 and S3 creates a barrier to folding. Left-handed crossovers between β-strands are very rare in proteins (*47*), and left-handed beta−alpha−beta crossovers have been reported to be of significantly higher energy than the common right-handed connections (*48*). Figure 5 shows the left-handed pitch of the crossover between β2 and β3 and, for comparison, the right-handed pitch of the crossover between β3 and β4.

To test whether proper insertion of the S3 β-strand creates a topological barrier to folding, we created a disulfide mutant (T22C, S87C), which links the ends of β-strand S1 and S3 (Figure 5). The disulfide does not eliminate the left-handed crossover but insures that the strand after the left-handed crossover (S3) is inserted in its native position between S1 and S2. Denatured T22C, S87C, and S221C subtilisin (2 μM) was refolded with an excess of proR9 (3.3−21 μM) in 30 mM Tris-HCl and 50 mM KCl at pH 7.4 at 25 °C. The folding reaction was followed after stopped flow mixing. The rates and amplitudes of fluorescence changes during a single turnover of subtilisin folding were measured. In contrast to the reaction without the cross-link, folding kinetics with the 22−87 disulfide bond have multiple kinetic phases (Figure 6) with an intermediate rapidly accumulating upon neutralization of the denatured protein. About 75% of T22C, S87C, S221C is rapidly bound to proR9. The remaining 25% apparently undergoes a slow step (0.015 s^{-1}) prior to binding. Assuming that the fast and slow binding fractions are at

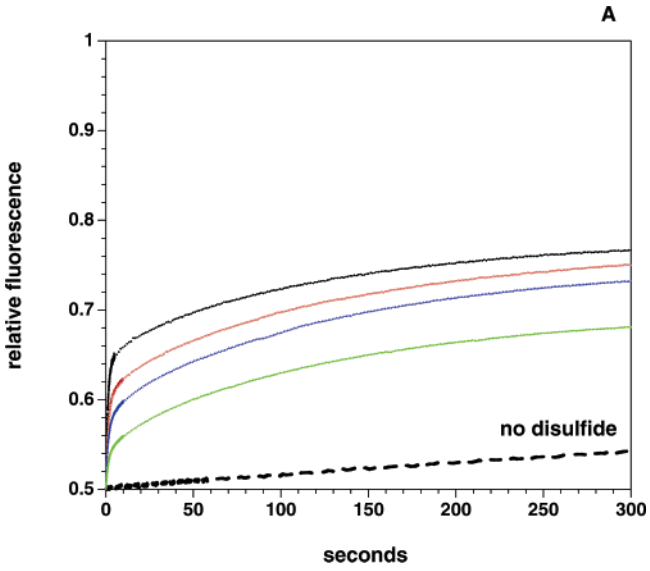

FIGURE 6: Folding rate of S22C, T87C, and S221C subtilisin in the presence of proR9. ProR9 and 1 μM denatured subtilisin were mixed in 30 mM Tris-HCl at pH 7.4 and 50 mM KCl at 25 °C. The reaction was followed by an increase in tryptophan fluorescence, which occurs upon the folding of subtilisin into the prodomain−subtilisin complex. The concentrations of proR9 were as follows: 3.3 μM, green; 5.6 μM, blue; 10 μM, red; and 21 μM, black. For comparison, the folding curve of S221A subtilisin without the cross-link and 20 μM proR9 is shown in black (---).

equilibrium prior to proR9 binding, the reverse rate (k_{-1}) would be 0.005 s^{-1}. The rate and amplitude of this minor phase is independent of proR9 concentration.

The major kinetic components were fit to a double exponential equation. The rate of the fast phase of the reaction versus proR9 concentration increases linearly with a slope of 2.1 $\times$ 10^4 M^{-1} s^{-1} and an intercept at 0.5 s^{-1} (Figure 7A). According to our model, the fast phase of the reaction corresponds to the formation of the initial collision complex PI (binding phase), and the slow phase corresponds to the decay of PI and the formation of PN (isomerization phase). The rate of the slow phase increases hyperbolically with proR9 concentration and reached a maximum rate of 0.0015 s^{-1}. Figure 7B shows the amplitudes of the fast and slow phases plotted versus proR9 concentration. This kinetic behavior can be fit using mechanism 3.

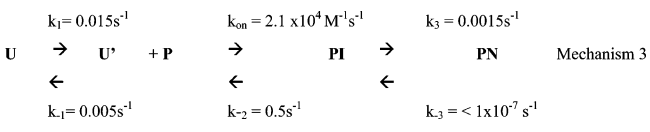

The major difference in the folding of subtilisin with the cross-link is that no slow conformational change in the unfolded state is required prior to proR9 binding for 75% of the unfolded protein. The disulfide also does not alter the rate of the isomerization step PI to PS nor does it result in folding in the absence of proR9. The primary kinetic effect of the cross-link is to shift the equilibrium for U (which does not bind proR9) toward U′ (which binds proR9 at a rate of 2.1 $\times$ 10^4 M^{-1} s^{-1}). As observed with A221 subtilisin, the rate constant k_{-3} is small and estimated from the H−D exchange data (the next article). This behavior is consistent with the idea that the left-handed crossover creates a kinetic block to forming the folding intermediate, which is relieved by cross-linking strands S1 and S3 in the native arrangement.

Left-Hand Crossover: Effect of the 75−83 Deletion. Previously, we created a mutant of subtilisin in which the calcium site A binding loop is deleted (Δ75-83) from helix C. The deletion eliminates calcium binding at the A-site and allows the folding reaction to be studied independent of calcium concentration. However, the 75−83 deletion facilitates folding in a manner that transcends the binding of calcium ions. Δ75-83 subtilisin folds even without added prodomain (k_{fold} = 0.0033 s^{-1}, 0.2 M KPO_2 at pH 7.2) (*49*). Subtilisin with the calcium loop is not observed to fold at all under similar conditions. The loop deletion appears to remove barriers to both the catalyzed and uncatalyzed folding reactions. Helix C is part of the left-handed crossover between β-strands 2 and 3; hence, the deletion shortens the crossover by nine amino acids. S221A, a Δ75-83 mutant (denoted sbt70), has been used as a folding model for subtilisin, and data on its structure, stability, and folding behavior have been previously reported (*37*, *41*). Its hydrogen exchanges rates in the presence and absence of proR9 are described in the next article.

Denatured Δ75-83, S221A subtilisin (1 μM), was refolded with an excess of proR9 (5−20 μM). The folding reaction was followed after stopped flow mixing. The rates and amplitudes of fluorescence changes during a single turnover of subtilisin folding were measured. The bimolecular folding reaction occurs in two steps: the binding of proR9 to unfolded subtilisin occurs at a rate of 1 $\times$ 10^5 M^{-1} s^{-1}, followed by a slow step with an observed rate of 0.15 s^{-1}. Figure 7A shows the rate of the binding phase versus proR9 concentration.

Role of Proline Isomerization in the PI to PN Folding Step. To investigate whether proline isomerization was involved in the folding of PI into the native complex, a double-jump experiment was designed to study the effect of denaturation time on the rates and amplitudes of the folding reaction (*50*, *51*). The sbt70 subtilisin mutant is particularly useful for this experiment because it can be rapidly denatured. Its rate of unfolding (30 s^{-1} at pH 2.1 (*37*)) is much faster than the rate of proline isomerization.

In the first mixing reaction, 3 μM sbt70 and 30 μM proR9 were denatured by mixing with acid, and the denaturation reaction was aged for varied lengths of time. The second mixing step returns the solution to neutral pH. The folding process is then followed by fluorescence change, and the rate and amplitude changes were determined at [proR9] = 10 μM. The folding reaction was fit to double-exponential equations. The rate of the fast and slow renaturation phases was constant with denaturation time, but the amplitude contributed by each phase changed as the denaturation time increased (Figure 8). The amplitude of the fast phase decreased at a rate of 0.06 s^{-1} before leveling out at about 80% of the total amplitude change, and the amplitude of the slow phase increased at a rate of 0.06 s^{-1} before leveling out at about 20% of the total amplitude change. From the experiment, we infer that there are two steps in the denaturation process. The faster step occurred at the rate of global unfolding (30 s^{-1}) and the slower step, not associated with any spectral changes in subtilisin, occurred at a rate of 0.06 s^{-1}.

These results suggest that the slow phase involves isomerization of prolyl peptide bonds in unfolded species (*52*). There are 14 proline residues in subtilisin. All but one

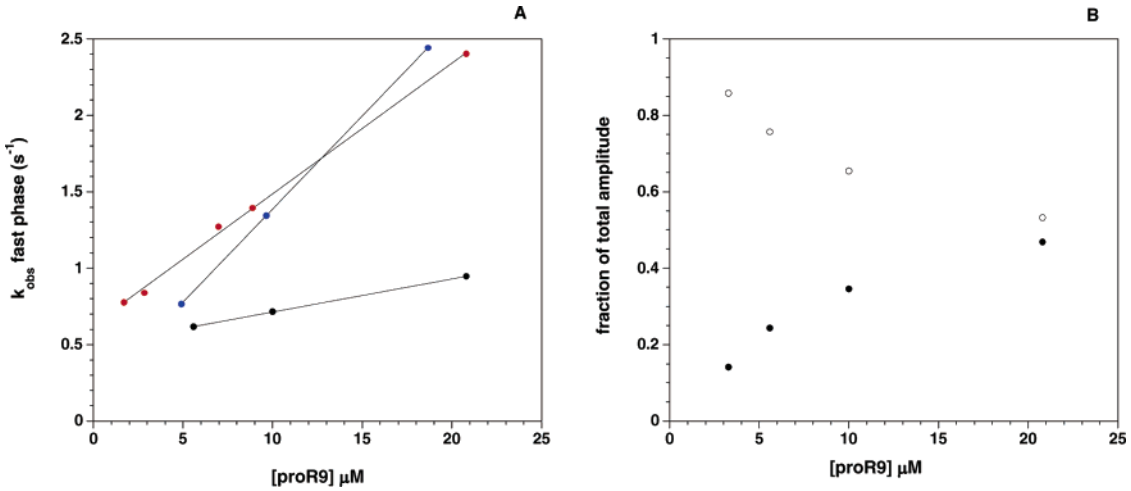

FIGURE 7: Refolding of subtilisin mutants in the presence of proR9. (A) Plot of the rates of the binding phases for S22C, T87C, and S221C subtilisin (black), sbt70 (blue) and D32N, and Δ75-83 subtilisin (red) as a function of proR9 in 30 mM Tris-HCl at pH 7.4 and 50 mM KCl at 25 °C. (B) Amplitudes of the fast phase (●) and slow phase (○) as a function of proR9 for S22C, T87C, and S221C subtilisin.

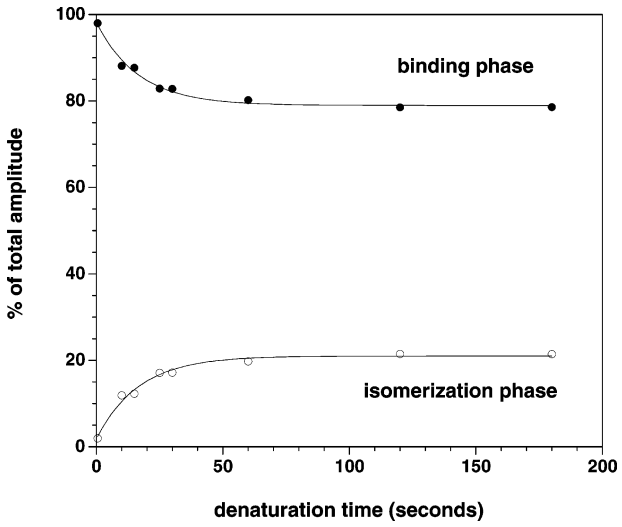

FIGURE 8: Measuring the rate of proline isomerization in the unfolded state of Sbt70 by double-jump denaturation−renaturation. Sbt70 was denatured in phosphoric acid for times ranging from 0.5 to 180 s. Samples were then renatured in 0.1 M KPi at pH 7.0 and 25 °C. The amplitudes of the fast and slow renaturation phases of the reaction are plotted as a function of denaturation time: ●, fast phase; ○, slow phase. Also shown is the single-exponential fit with a rate constant of 0.06 s^{-1} for both phases.

(Pro168) exist as trans isomers in the native structure (*34*). The peptide bond between proline and its preceding amino acid (Xaa−Pro bonds) exists as a mixture of cis and trans isomers in solution unless structural constraints such as those in folded proteins stabilize one of the two isomers. In the absence of ordered structure, the trans isomer is favored slightly over the cis isomer. The isomerization trans ⇔ cis is an intrinsically slow reaction with rates at 0.1 to 0.01 s^{-1} at 25 °C (*50*). Upon acid denaturation of subtilisin, the structural constraints are removed, and the trans and cis isomers of all 14 prolyl peptide bonds gradually come to equilibrium in the unfolded state, resulting in 2^{14} different proline isomer combinations. The fact that the rate of the fast phase of the reaction remains constant as a function of denaturation time shows that the rate of the initial binding reaction of proR9 with unfolded subtilisin is not influenced by the isomerization state of prolines.

Measuring the Accumulation of the Folded Complex at Short Denaturation Time. To study the catalyzed folding rate of subtilisin in the absence of prolyl peptide bond isomerization, folding kinetics were measured after a denaturation time of 0.5 s. The short denaturation time minimizes the amount of prolyl peptide bond isomerization occurring during the time required to unfold sbt70. After the 0.5 s denaturation step, the folding process was recorded as fluorescence increase versus time (Figure 9A). The refolding condition was 30 mM Tris-HCl at pH 7.4, at 25 °C, with 0.5 μM sbt70 and proR9 concentration = 5, 10, or 20 μM. At all three concentrations of proR9, folding kinetics are first order. The observed rate of folding increases as the concentration of proR9 increased and follows a linear relationship. The slope of the pseudo-first-order rate constants versus proR9 concentration yielded $k_{obs} = 1 \times 10^5$ M^{-1} s^{-1} (Figure 9B).

In order to prove that the fast kinetics observed above represents complete refolding to the native complex, we performed a triple mixing experiment to directly measure the accumulation of the native complex. Sbt70 was denatured for 0.5 s in the first mixing step and then refolded with proR9 in 30 mM Tris-HCl at pH 7.4 and 25 °C for different aging times in the second mixing step. In the third mixing step, the folding reaction was denatured in phosphoric acid, and the amplitude change of fluorescence was recorded as a function of refolding time. Figure 9A shows the results of the triple-jump experiment using 5 μM proR9. The fraction of the folded complex is plotted versus the time of renaturation. Also shown is the parallel double-jump experiment in which the fluorescence change is recorded during folding in 30 mM Tris-HCl and 5 mM KPi at pH 7.5. Both sets of data can be fit to a single-exponential equation with a rate constant of 0.4 s^{-1}. This demonstrates that by denaturing sbt70 just long enough so that unfolding was complete but prolyl peptide bond isomerization was negligible, the folding of the denatured subtilisin followed fast single-exponential kinetics. No intermediate was detectible in the course of the reaction because the formation of PN from PI is faster than the formation of the initial collision complex PI from P and U. Further details of the folding mechanism of Δ75-83 A221 subtilisin have been presented by Ruan et al. (*37*).

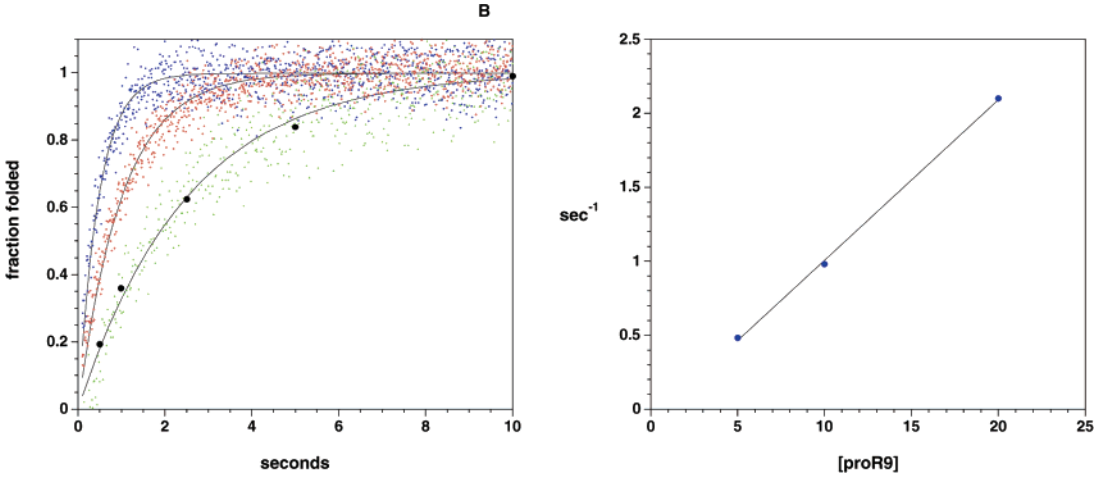

FIGURE 9: Folding kinetics of sbt70 after a short denaturation time. (A) Refolding kinetics of sbt70 were determined after 0.5 s of denaturation (small dots) using a double-jump denaturation−renaturation procedure as described in the text; [pror9] = 5 μM, green; 10 μM red; 20 μM blue. Also shown is the accumulation of PS after 0.5 s of denaturation (●), as measured in a triple-jump denaturation−renaturation−denaturation experiment at [proR9] = 5 μM. (B) Plot of first-order rate constants from part A vs [proR9] (slope = 1×10^5 M^{-1} s^{-1}).

For the purpose of comparison with other mutants analyzed in this study, the folding reaction of sbt70 from an unfolded state (U) with fully scrambled proline isomers is modeled according to mechanism 4, where PI is proR9 complexed with partially folded subtilisin with non-native proline isomers, and PI′ is proR9 complexed with partially folded subtilisin with all native proline isomers.

$$\begin{array}{lcccccccc} & & k_1 = 1\times10^5\ M^{-1}s^{-1} & & k_2 = 0.03s^{-1} & & k_3 > 3s^{-1} & & \\ U & + & P & \rightleftarrows & PI & \rightleftarrows & PI' & \rightleftarrows & PN \\ & & k_{-1} = 0.05\ s^{-1} & & k_{-2} = 0.16\ s^{-1} & & k_{-3} = <1\times10^{-7}\ s^{-1} & & \end{array} \qquad \text{Mechanism 4}$$

The deletion increases proR9 binding to U (k_1/k_{-1}) and accelerates the isomerization rate of PI to PN. In fact, the independent stability of I is sufficient to initiate folding even in the absence of the prodomain (*53*). The deletion also removes kinetic impediments to proR9 binding to the unfolded state so that no U′ form of the unfolded state accumulates. It is important to note here that the rate of proR9 binding to U is independent of the proline isomerization state. We believe that the major effect of the deletion is to stabilize helix C. When the 75−83 loop is present, stabilization of helix C is dependent on calcium binding to site A. Because site A cannot form until most of the tertiary structure is accumulated, the stability of helix C is compromised early in folding. The stability of helix C affects both the ability to bind the prodomain in the bimolecular intermediate and the ability of the bimolecular intermediate to further propagate folding.

Further Investigation into the Isomerization of PI to PN: P168G Mutation. Because a cis-peptide bond occurs between Y167 and P168, we hypothesized that the trans to cis isomerization of P168 might be largely responsible for the slow isomerization of PI to PN. To test this hypothesis, we mutated *cis*-proline 168 to glycine. Glycine at 168 resulted in only a small increase (1.5-fold) in the rate of the isomerization phase, however, compared to that of proline at 168. The mutation weakened the intermediate complex by about 4-fold (k_2 is similar but k_{-2} is faster by about 4-fold) (data not shown). The weaker binding of proR9 to the mutant may be because P168 creates part of the substrate-binding pocket. We conclude, therefore, that although prolines are the limiting factor in isomerization to the native state, *cis*-proline 168 does not play a larger role than other prolines.

Influence of D32 on the Folding Reaction. As alluded to earlier, the D32N mutant of subtilisin does not fold in a bimolecular reaction with proR9. This observation indicates that D32 forms critical interactions during folding. We introduced the D32N mutation into sbt70 so that we could observe folding in a facile-folding mutant. The folding reaction was followed using 1 μM denatured D32N, Δ75-83 subtilisin, and varied proR9 concentrations. The folding reaction is distinctly biphasic (data not shown). Plotting the rate of the fast phase of the reaction versus proR9 concentration results in a straight line with a slope of 8.5×10^4 M^{-1} s^{-1} (Figure 7A) and an intercept at 0.6 s^{-1}. The intercept defines the decay of PI and is equal to ($k_{-1} + k_2$). The amplitude of the fast phase increased as proR9 concentration increased and leveled off at 85% of the total fluorescence change at [proR9] > 40 μM. The amplitude of the slow phase decreased with increasing proR9 concentration, and leveled off at 15% at [proR9] > 40 μM. The total amplitude change is independent of proR9 concentration. The fast phase of the reaction corresponds to the formation of the initial collision complex PI (binding phase), and the slow phase corresponds to the formation of PN from PI (isomerization phase). The rate of the slow phase of the reaction increased with proR9 concentration and leveled off at 0.007 s^{-1} at [proR9] > 40 μM. The behavior is qualitatively similar to the folding of the corresponding Δ75-83 subtilisin with wild type D32, except that the binding of proR9 to the intermediate is weaker by about 10-fold, and the isomerization of PI to PN is slower by 25-fold. Thus, the mutation of D32N weakens both the binding of proR9 to the intermediate and disrupts the interactions that facilitate the isomerization of PI to PN. The effects of D32N and Δ75-83 can be accommodated in mechanism 2 as follows.

$$\begin{array}{lcccccc} & & k_1 = 8.5\times10^4 M^{-1}s^{-1} & & k_2 = 0.007s^{-1} & & \\ U & + & P & \rightleftarrows & PI & \rightleftarrows & PN \\ & & k_{-1} = 0.6\ s^{-1} & & k_{-2} = <1\times10^{-7}\ s^{-1} & & \end{array} \qquad \text{Mechanism 5}$$

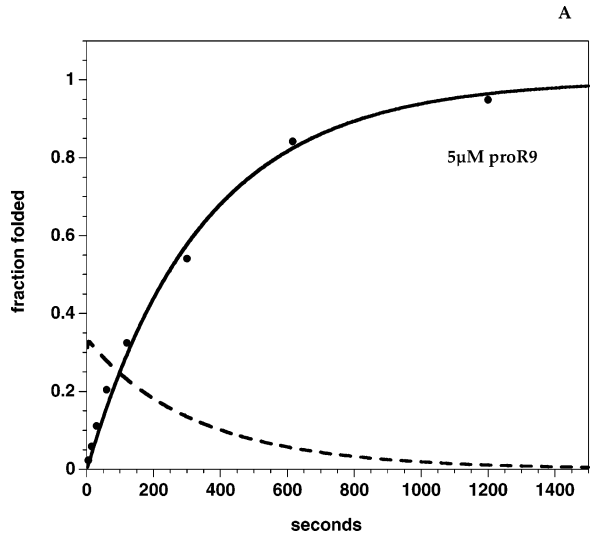

FIGURE 10: Accumulation of the folded complex by double-jump renaturation−denaturation: 1 μM denatured D32N and Δ75-83 subtilisin and 5 μM proR9. The denatured protein was returned to native conditions (30 mM Tris-HCl at pH 7.4 and 50 mM KCl at 25 °C) and allowed to fold for aging times from 10 to 1500 s. In the second step, the aged mixture was mixed with phosphoric acid, bringing the sample to pH 2.1. The amplitude of the denaturation reaction is determined for each aging time to determine how much folded complex has accumulated. The solid circles show the accumulation of PS. Also shown is the KINSIM (*55*) simulation of PI as a function of folding time using the rate constants given in the text.

To verify the mechanism, a double-jump renaturation−denaturation experiment was used to directly monitor the rate of accumulation of the fully folded complex (*54*). In the first mixing step, 1.5 μM unfolded subtilisin is mixed with an excess amount of proR9 in the folding buffer, 30 mM Tris-HCl and 5 mM KPi at pH 7.5 and 25 °C. The folding mixture is aged for varied lengths of time. In the second mixing step, the aged mixture is denatured by mixing with phosphoric acid, with a final pH of 2.1. Thus, by measuring the fluorescence amplitude of acid denaturation as a function of the aging time of the folding reaction, we were able to monitor the accumulation of the folded complex. The double jump data were plotted as a fraction of PS versus folding time. Figure 10 shows the rate of accumulation of PS as a function of folding time in 5 μM proR9 and the simulated curves calculated according to mechanism 5.

CONCLUSIONS

The goal of this work was to determine why subtilisin does not fold without the prodomain and to determine how the prodomain overcomes the kinetic barriers. Folding proceeds through one major intermediate, which forms early in the folding process and is stabilized by prodomain binding. The folding of the bimolecular intermediate into the native complex involves multiple proline isomerizations, which allow the formation of cation binding sites. The inordinately slow folding of subtilisin results from the accrued effects of two barriers. The first barrier to folding is the low stability of nascent structures. Ordinarily, a thermodynamically stable native state is sufficient to ensure an efficient folding pathway through stable, partially folded states. Native subtilisin is thermodynamically unstable in the absence of bound metals. Because the two metal binding sites are formed late in folding, they contribute little to the stability of folding intermediates. Added to this is the topological challenge of forming a left-handed crossover connection. The left-handed excursion is required for insertion of the S3 β-strand between S1 and S2 and is required to propagate the folding reaction. Helix C is the principal structural component of the crossover connection and is an interlocking part of the final native structure. It is interlaced with the 202−219 β-hairpin, the 33−43 ω-loop connecting β-strands S1 and S2, and the central β-sheet (Figure 5). When the native calcium site A loop is present, the independent stability of helix C appears to be compromised. Thus, to form the critical intermediate, the unfavorable left-handed excursion between the β-strands S2 and S3 must be made without the benefit of stabilizing interactions from elsewhere in the molecule. This serious topological challenge can be mitigated by deletion of the 75−83 loop, which increases the independent stability of helix C, or by the presence of the 22−87 disulfide cross-link, which ensures the native arrangement of β-strands S1 and S3. The disulfide accelerates the formation of the bimolecular intermediate but does not facilitate its isomerization to the native complex. The Δ75-83 mutation does both. This indicates the critical role of helix C in both parts of the reaction. The importance of helix C is also seen by the effect of the D32N mutation, which eliminates the strong hydrogen bond between D32 in β-strand S1 and H64 in helix C. The loss of this H-bond destabilizes PI and slows its isomerization to PN.

The second barrier slowing the folding reaction is a requirement for proline isomerization late in the folding process. Rate-limiting proline isomerization is common in protein folding, but its effect in slowing subtilisin folding is amplified because of the instability of the intermediate. Furthermore, we would suggest that a heightened barrier between PI and PN is created by the need for simultaneous isomerization of multiple prolines into their native conformations in order to create metal site B. The formation of the bimolecular intermediate depends on neither the isomerization state of prolines nor the binding of ions. The final acquisition of the native structure depends on both, however. At low metal concentration, the bimolecular complex is stable but does not fold to the native state because metal binding is required to pull the equilibrium to the native conformation. Although there is no direct evidence to implicate particular prolines as being key in the late folding transition, we point out that the formation of site B requires prolines 168, 172, and 194 to be in their native isomeric forms. Without all being in the native conformation (168-cis, 172-trans, 194-trans) no stabilization from metal binding at site B is realized. ProR9 binding appears to stabilize the site B loops and increase the probability that all three prolines simultaneously occur as native isomers. Support for this hypothesis is presented in the next article on residue-specific H−D exchange.

In summary, the slow folding of subtilisin results from the accrued effects of the two slow and sequential processes: (1) the formation of an unstable and topologically challenged intermediate and (2) the proline-limited isomerization of the intermediate to the native state. The next article will present further structural explanation of the role of proR9 in the folding reaction from H−D exchange studies of subtilisin in the free and complexed forms.

ACKNOWLEDGMENT

We thank Edward Eisenstein and John Moult for helpful discussions.

REFERENCES

1. Khan, A. R., and James, M. N. (1998) Molecular mechanisms for the conversion of zymogens to active proteolytic enzyme, *Protein Sci. 7*, 815−836.
2. Baker, D., and Agard, D. (1994) Kinetics versus thermodynamics in protein folding, *Biochemistry 33*, 7505−7509.
3. Sohl, J. L., Jaswal, S. S., and Agard, D. A. (1998) Unfolded conformations of alpha-lytic protease are more stable than its native state, *Nature 395*, 817−819.
4. Bryan, P. N. (2002) Prodomains and protein folding catalysis, *Chem. Rev. 102*, 4805−4816.
5. Wells, J. A., et al. (1983) Cloning, sequencing and secretion of *Bacillus amyloliquifaciens* subtilisin in *Bacillus subtilis*, *Nucleic Acids Res. 11*, 7911−7925.
6. Vasantha, N., et al. (1984) Genes for alkaline and neutral protease from *Bacillus amyloliquifaciens* contain a large open-reading frame between the regions coding for signal sequence and mature protein, *J. Bacteriol. 159*, 811−819.
7. Wong, S., and Doi, R. (1986) Determination of the signal peptide cleavage site in the preprosubtilisin of *Bacillus subtilis*, *J. Biol. Chem. 261*, 10176−10181.
8. Power, S. D., Adams, R. M., and Wells, J. A. (1986) Secretion and autoproteolytic maturation of subtilisin, *Proc. Natl. Acad. Sci. U.S.A. 83*, 3096−3100.
9. Ikemura, H., Takagi, H., and Inouye, M. (1987) Requirement of pro sequence for the production of active subtilisin in *Escherichia coli*, *J. Biol. Chem. 262*, 7859−7864.
10. Baker, D., Sohl, J. L., and Agard, D. A. (1992) A protein-folding reaction under kinetic control, *Nature 356*, 263−265.
11. Silen, J. L., and Agard, D. A. (1989) The alpha-lytic protease pro-region does not require a physical linkage to activate the protease domain *in vivo*, *Nature. 341*, 462−464.
12. Zhou, A., Bloomquist, B. T., and Mains, R. E. (1993) The prohormone convertases PC1 and PC2 mediate distinct endoproteolytic cleavages in a strict temporal order during proopiomelanocortin biosynthetic processing, *J. Biol. Chem. 268*, 1763−1769.
13. Baier, K., et al. (1996) Evidence for propeptide-assisted folding of the calcium-dependent protease of the cyanobacterium *Anabaena*, *J. Eur. Biochem. 241*, 750−755.
14. Fabre, E., et al. (1991) Role of the proregion in the production and secretion of the *Yarrowia lipolytica* alkaline extracellular protease, *J. Biol. Chem. 266*, 3782−3790.
15. Fabre, E., Tharaud, C., and Gaillardin, C. (1992) Intracellular transit of a yeast protease is rescued by trans-complementation with its prodomain, *J. Biol. Chem. 267*, 15049−15055.
16. Chang, Y. C., et al. (1996) Secretion of active subtilisin YaB by a simultaneous expression of separate pre-pro and pre-mature polypeptides in *Bacillus subtilis*, *Biochem. Biophys. Res. Commun. 219*, 463−468.
17. Baardsnes, J., et al. (1998) Streptomyces griseus protease B: secretion correlates with the length of the propeptide, *J. Bacteriol. 180*, 3241−3244.
18. Steiner, D., et al. (1992) The new enzymology of precursor processing endoproteases, *J. Mol. Biol. 267*, 23435−23438.
19. Holyoak, T., et al. (2003) 2.4 Å resolution crystal structure of the prototypical hormone-processing protease Kex2 in complex with an Ala-Lys-Arg boronic acid inhibitor, *Biochemistry 42*, 6709−6718.
20. Henrich, S., et al. (2003) The crystal structure of the proprotein processing proteinase furin explains its stringent specificit, *Nat. Struct. Biol. 10*, 520−526.
21. Tangrea, M. A., et al. (2001) Stability and global fold of the mouse prohormone convertase 1 pro-domain, *Biochemistry 40*, 5488−5495.
22. Tangrea, M. A., et al. (2002) Solution structure of the pro-hormone convertase 1 pro-domain from *Mus musculus*, *J. Mol. Biol. 320*, 801−812.
23. van den Hazel, H. B., Kielland-Brandt, M. C., and Winther, J. R. (1993) The propeptide is required for in vivo formation of stable active yeast proteinase A and can function even when not covalently linked to the mature region, *J. Biol. Chem. 268*, 18002−18007.
24. Cawley, N. X., et al. (1998) Activation and processing of non-anchored yapsin 1 (Yap3p), *J. Biol. Chem. 273*, 584−591.
25. Fukuda, R., et al. (1994) The prosequence of *Rhizopus niveus* aspartic proteinase-I supports correct folding and secretion of its mature part in *Saccharomyces cerevisiae*, *J Biol. Chem. 269*, 9556−9561.
26. Nirasawa, S., et al. (1999) Intramolecular chaperone and inhibitor activities of a propeptide from a bacterial zinc aminopeptidase, *J. Biochem. 341*, 25−31.
27. Marie-Claire, C., et al. (1999) The prosequence of thermolysin acts as an intramolecular chaperone when expressed in trans with the mature sequence in *Escherichia coli*, *J. Mol. Biol. 285*, 1911−1915.
28. Cao, J., et al. (2000) The propeptide domain of membrane type 1-matrix metalloproteinase acts as an intramolecular chaperone when expressed in trans with the mature sequence in COS-1 cells, *J. Biol. Chem. 275*, 29648−29653.
29. Ventura, S., et al. (1999) Mapping the pro-region of carboxypeptidase B by protein egineering cloning, overexpression, and mutagenesis of the porcine proenzyme, *J. Biol. Chem. 274*, 19925−19933.
30. Wetmore, D. R., and Hardman, K. D. (1996) Roles of the propeptide and metal ions in the folding and stability of the catalytic domain of stromelysin (matrix metalloproteinase 3), *Biochemistry 35*, 6549−6558.
31. Yamamoto, Y., et al. (1999) Proregion of *Bombyx mori* cysteine proteinase functions as an intramolecular chaperone to promote proper folding of the mature enzyme, *Arch. Insect Biochem. Physiol. 42*, 167−178.
32. Gallagher, T. D., et al. (1995) The prosegment-subtilisin BPN′ complex: crystal structure of a specific foldase, *Structure 3*, 907−914.
33. Jain, S. C., et al. (1998) The crystal structure of an autoprocessed Ser221Cys-subtilisin E-propeptide complex at 2.0 Å resolution, *J. Mol. Biol. 284*, 137−144.
34. McPhalen, C. A., and James, M. N. G. (1988) Structural comparison of two serine proteinase-protein inhibitor complexes: eglin-C-subtilisin Carlsberg and CI-2-subtilisin novo, *Biochemistry 27*, 6582−6598.
35. Alexander, P. A., Ruan, B., and Bryan, P. N. (2001) Cation-dependent stability of subtilisin, *Biochemistry 40*, 10634−10639.
36. Pantoliano, M. W., et al. (1988) The engineering of binding affinity at metal ion binding sites for the stabilization of proteins: subtilisin as a test case, *Biochemistry 27*, 8311−8317.
37. Ruan, B., Hoskins, J., and Bryan, P. (1999) Rapid folding of calcium-free subtilisin by a stabilized pro-domain mutant, *Biochemistry 38*, 8562−8571.
38. Strausberg, S. L., et al. (2005) Directed coevolution of stability and catalytic activity in calcium-free subtilisin, *Biochemistry 44*, 3272−3279.
39. Bryan, P. N., (2004) Dynamics and Mechanism of Protein Folding: Protein Folding Catalysis by Pro-Domains, in *Protein Folding Handbook* (Buchner, J., and Kiefhaber, T., Eds.) pp 1028−1054, Wiley-VCH, Weinheim, Germany.
40. Alexander, P., et al. (1992) Thermodynamic analysis of the folding of the streptococcal protein G IgG-binding domains B1 and B2: why small proteins tend to have high denaturation temperatures, *Biochemistry 31*, 3597−3603.
41. Bryan, P., et al. (1995) Catalysis of a protein folding reaction: mechanistic implications of the 2.0 Å structure of the subtilisin-prodomain complex, *Biochemistry 34*, 10310−10318.
42. Eder, J., Rheinnecker, M., and Fersht, A. R. (1993) Folding of subtilisin BPN′: role of the pro-sequence, *J. Mol. Biol. 233*, 293−304.
43. Ruan, B., et al. (1998) Stabilizing the subtilisin BPN′ pro-domain by phage display selection: how restrictive is the amino acid code for maximum protein stability? *Protein Sci. 7*, 2345−2353.
44. Kuhn, P., et al. (1998) The 0.78 Å structure of a serine protease: *Bacillus lentus subtilisi*, *Biochemistry 37*, 13446−13452.
45. Bryan, P., et al. (1986) Site-directed mutagenesis and the role of the oxyanion hole in subtilisin, *Proc. Natl. Acad. Sci. U.S.A. 83*, 3743−3745.
46. Day, R. M., et al. (2003) Tautomerism, acid-base equilibria, and H-bonding of the six histidines in subtilisin BPN′ by NMR, *Protein Sci. 12*, 794−810.
47. Richardson, J. S. (1976) Handedness of crossover connections in beta sheets, *Proc. Natl. Acad. Sci. U.S.A. 73*, 2619−2623.

48. Chou, K. C., et al. (1989) Energy of stabilization of the right-handed beta alpha beta crossover in proteins, *J. Mol. Biol. 205*, 241−249.
49. Bryan, P. N. (1995) Subtilisin Engineered for Facile Folding: Analysis of Uncatalyzed and Prodomain-Catalyzed Folding, in *Intramolecular Chaperones and Protein Folding* (Shinde, U., and Inouye, M., Eds.) pp 85−112, R. G. Landes, Austin, TX.
50. Brandts, J. F., Halvorson, H. R., and Brennan, M. (1975) Consideration of the possibility that the slow step in protein denaturation reactions is due to cis-trans isomerism of proline residues, *Biochemistry 14*, 4953−4963.
51. Kiefhaber, T. and Schmid, F. X. (1992) Kinetic coupling between protein folding and prolyl isomerization. II. Folding of ribonuclease A and ribonuclease T1, *J. Mol. Biol.*, 231−240.
52. Eyles, S. J., and Gierasch, L. M. (2000) Multiple roles of prolyl residues in structure and folding, *J. Mol. Biol. 301*, 737−747.
53. Bryan, P., et al. (1992) Energetics of folding subtilisin BPN′, *Biochemistry 31*, 4937−4945.
54. Kiefhaber, T. (1995) Kinetic traps in lysozyme folding, *Proc. Natl. Acad. Sci. U.S.A. 92*, 9029−9033.
55. Barshop, B. A., Wrenn, R. F., and Frieden, C. (1983) Analysis of numerical methods for computer simulation of kinetic processes: development of KINSIM−a flexible, portable system, *Anal. Biochem. 130*, 134−145.

BI061600Z